

pubs.acs.org/JPCC Article

# Insight into the Adsorption Structure of TIPS-Pentacene on Noble Metal Surfaces

Brian Breeman, Angelo T. Tiglias, Joseph Mancuso, Eva Zurek, Daniel P. Miller,\* and Luis Velarde\*



Cite This: J. Phys. Chem. C 2022, 126, 2689–2698



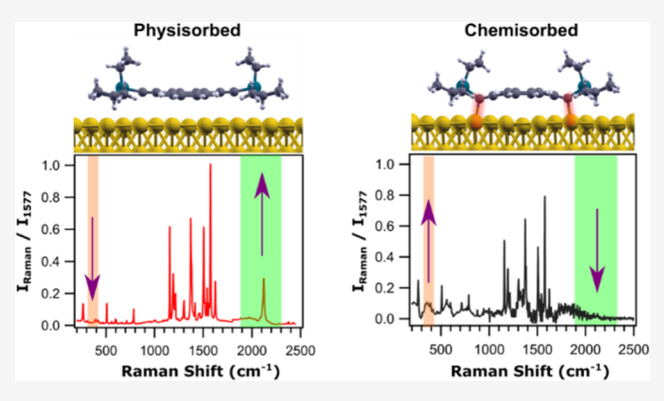
**ACCESS** 

Metrics & More

Article Recommendations

Supporting Information

ABSTRACT: Organic—metal interfaces are of vital importance for regulating the optoelectronic properties of devices in molecular electronics. Interactions within the metal—adsorbate system influence the photonic performance through perturbations of the electronic structure. Such changes and associated interfacial charge transfer are directly influenced by how the organic molecule structurally adsorbs to the substrate. Herein, we use a combination of surface-enhanced Raman scattering (SERS) spectroscopy and dispersion-corrected density functional theory (DFT-D) to show that 6,13-bis(triisopropylsilylethynyl)pentacene (TIPS-Pc) adsorbs through both physisorption and chemisorption on a gold surface with the TIPS-Pc adopting an adsorption geometry with the pentacene backbone oriented parallel to the substrate. When



chemisorbed, our results provide direct evidence of Au–C bond formation within the ethynyl moieties. Most importantly, we demonstrate that the electronic structure of the resulting TIPS-Pc surface system is distinctly dependent on the adsorption mechanism. These results show new evidence of chemisorption routes for TIPS-Pc on metal surfaces and illustrate the importance of understanding the interfacial structure at the molecular level for dictating and assessing the performance of molecular optoelectronic devices.

#### ■ INTRODUCTION

Molecular adsorption at the metal-organic interface is one of the fundamental aspects of heterogeneous chemistry. 1,2 Heterogeneous chemistry lays the foundation for several fields, including molecular electronics and heterogeneous catalysis.<sup>2</sup> The exact nature of molecular adsorption to metal surfaces plays a crucial role in these disciplines. For instance, molecules can adsorb to a surface covalently via chemisorption or noncovalently via physisorption. 5-7 The strength of adsorbate-surface versus adsorbate-adsorbate interactions determines the preferential adsorption mechanism.<sup>8,9</sup> Previous literature has shown that adsorption, being chemisorption versus physisorption, determines whether Pt(111) is chemically reactive toward dissociation of molecular oxygen. 10,11 Moreover, work by Wodtke and co-workers has shown how molecular vibrations can be used to reveal the intricate interplay between physisorption and chemisorption states that strongly influence the surface chemistry.<sup>2,12</sup>

One particular class of molecules that has provided an exciting new area for molecular electronics is singlet fission organic chromophores. Singlet fission chromophores can exhibit inordinately high quantum efficiencies per photoelectric event via the process of singlet fission, namely, the process of converting a singlet exciton into two triplet excitons intermolecularly. This process is basically the reverse of triplet—triplet annihilation in multi-excitonic systems such as

quantum dots.<sup>20</sup> Although the exact mechanism is still under debate, some of the fundamental requirements are well established. First, the singlet excitation energy must be roughly double that of the triplet. 19 Second, there must be a neighboring moiety in the ground state with the appropriate orbital overlap to accept energy from the exciton (either in dimers or monomer pairs). 19 Most literature studies on these materials focus on acenes, such as pentacene and their derivatives, 14,18,19,21,22 rubrene, 23-25 and perylene diimides.<sup>26-28</sup> Most of these studies are either in the solution phase or in single/polycrystalline phases and investigate elementary charge transfer and electronic processes of these materials, <sup>29-31</sup> assisted by related computational studies. <sup>32,33</sup> In application, however, these chromophores are often in single or polycrystalline thin films, <sup>19,34–36</sup> and characterization of their properties at interfaces and within thin films becomes essential. For instance, substrate choice and temperature can be used as a control for the pentacene phase and orientation in a film.3

Received: December 3, 2021 Revised: January 12, 2022 Published: January 28, 2022





Therefore, the adsorption of molecules on solid surfaces can alter the chemistry of these organic molecules, especially on metal surfaces, underscoring the significance of understanding the strength of the adsorbate—substrate interactions (along with lateral adsorbate—adsorbate interactions) for determining molecular orientation, structure and growth and how the adsorption geometry defines the electronic structure of the adsorbate—substrate system.

Herein, we examine the adsorption of 6,13-bis-(triisopropylsilylethynyl)pentacene (TIPS-Pc), an organic semiconductor and one of the most popular pentacene derivatives, on gold (Au) surfaces. The Au substrate has been selected due to its wide use as an electrode in electronic devices and previous TIPS-Pc/gold studies on singlet fission and optoelectronics.<sup>38–41</sup> On Au(111), angle-resolved near-edge Xray absorption fine structure<sup>38</sup> and vibrational high-resolution electron energy loss spectroscopy<sup>39</sup> measurements suggested a rather parallel physisorption of the acene plane relative to the surface, and a slight incline was suggested. Our theoretical calculations, however, deduce that chemisorption of TIPS-Pc can also occur through breaking the alkyne bond into an alkene to then form an Au-C bond. Our density functional theory (DFT) computations suggest that this is energetically the most stable adsorption mechanism, although this is only possible when the active carbons are placed above the top sites on the gold surface. Surface-enhanced Raman scattering (SERS) experiments of saturated and submonolayer-covered TIPS-Pccoated gold nanorods support the theoretical results. Finally, the presence of both chemisorption and physisorption is discussed more broadly as these adsorption motifs alter the electronic structure of the system, with potential ramifications toward the effect of singlet fission.

#### METHODS

Thin-Film Sample Preparation. Gold substrates were purchased from EMF Corp., consisting of microscope slides coated with a 50 Å binder layer of titanium followed by deposition of a 100 nm bare gold (Au) layer with no protective overcoat. The substrates are cleaned in the following way to remove all organic and inorganic contamination from the surface. 42 First, the gold substrates were sonicated in acetone for 20 min and rinsed in 18.2 M $\Omega$  cm<sup>-1</sup> nanopure water, followed by sonication in Alconox detergent (10% in nanopure water) for 20 min and rinsing again with nanopure water and sonication for 20 min in only 18.2 M $\Omega$  cm<sup>-1</sup> ultrapure water with subsequent rinsing. Upon completion of these rinses, excess moisture was removed by ultra-high purity N<sub>2</sub> gas flow and dried in an oven at 110 °C under ambient conditions to completely dehydrate it. Dried substrates were then sanitized in a UV/ozone cleaner for 2 h. This same procedure was utilized for cleaning the silica substrates. The gold layer on the substrates appears to be resistant to the cleaning procedure, leaving the Au layer mostly unaffected even after ultrasonification, heating to ~110 °C, and exposure to ultraviolet light, while effectively removing all trace organics from the surface. However, surface roughness measurements before and after cleaning were not taken due to limited number of available substrates. It has been reported that heating in this temperature range may induce slight grain boundary motion to reduce the surface roughness.<sup>43</sup> TIPS-Pc was purchased from Sigma-Aldrich and used as received. Solutions of 5.7 mM TIPS-Pc in chloroform were prepared, allowing for solution processed film fabrication via drop casting. In all cases, substrates were tilted

between roughly 3 and  $10^\circ$  to maximize homogeneity and limit macroscopic aggregation at the edges of the substrate. Upon drop casting, TIPS-Pc droplets settled for 15 min for complete solvent evaporation. There were no signs of delamination or cracking of the substrate surfaces (as observed through a Renishaw Raman microscope as discussed below) caused by the brief exposure to chloroform. All TIPS-Pc films are expected to maintain a thickness between 200 and 800 nm according to previous reports.  $^{44}$ 

Raman Spectroscopy/SERS. All Raman measurements taken of TIPS-Pc on gold utilized a Renishaw inVia microscope with an objective magnification of  $50\times$ . The excitation wavelength used to perform this study was 785 nm because it is pre-resonant with all electronic transitions of TIPS-Pc in the solid-state films. The grating was 1200 L/m, and spectra were acquired for 3 min in 10 s accumulations within a spectral range of 200 to 2300 cm<sup>-1</sup> with switching between various vibrational regions. All spectra presented are the average of Raman spectra acquired in triplicate.

To perform the SERS studies, 1 optical density (O.D.) citrate-capped gold nanorods with a width of 10 nm and length of 44 nm were purchased from Nanocomposix. The plasmon resonance for the long axis of the nanorods was centered at 800 nm (Figure S13 in the Supporting Information), so the excitation wavelength of 785 nm was well within the plasmon band. The nanorod solution was drop-cast on a glass slide cleaned using the procedure above and treated with UV/ozone for 15, 30, and 60 min to remove the citrate capping ligand. From there, the 5.7 mM TIPS-Pc solution was drop-cast on the nanorod film. To exclude the concern of potential aggregation, we also prepared samples using this procedure with a 0.5  $\mu$ M solution instead. All instrument parameters were kept identical between the SERS and Raman experiments. All data were processed using Igor Pro 8 software with all peaks being fit to Lorentzian distributions.

**Computational Details.** Dispersion-corrected DFT (DFT-D) calculations were performed with VASP<sup>45</sup> to obtain binding energies (BEs) for TIPS-Pc to Au(111) surfaces through geometry optimizations. The revPBE (revised Perdew–Burke–Ernzerhof) GGA functional<sup>46,47</sup> with the Grimme3<sup>48</sup> dispersion correction was used with a Monkhorst–Pack<sup>49</sup> (3 × 3 × 1) k-grid for all TIPS-Pc to Au(111)-adsorbed systems. A planewave basis set of 500 eV was used. The projector augmented wave method<sup>50,51</sup> was employed to treat the core states. All atoms were allowed to relax fully within the surface–adsorbate geometry optimizations, except for the bottom two layers of the four-layer Au(111) slabs. The computed bulk lattice constant of 4.138 Å was chosen to model the Au surfaces. All BEs were calculated as follows:

$$BE = E_{\text{surface-adsorbate}} - E_{\text{adsorbate}} - E_{\text{surface}}$$

The charge density difference (CDD) isosurfaces<sup>52</sup> were obtained in a similar fashion to that of the BE but by using respective charge densities instead of energies. Furthermore, DFT-D calculations were performed with the ADF<sup>53</sup> software package. The revPBE-D3<sup>46-48</sup> functional and dispersion correction, along with a TZP basis set,<sup>54</sup> were used to obtain IR and Raman vibrational spectra for a simplified TIPS-Pc model adsorbed to an Au surface. In all other surface—adsorbate calculations, a full four-layer Au(111) surface and TIPS-Pc with its isopropyl groups were used. The core electrons were frozen, and the relativistic scalar ZORA<sup>56</sup> method was used as Au exhibits relativistic effects. In the IR and

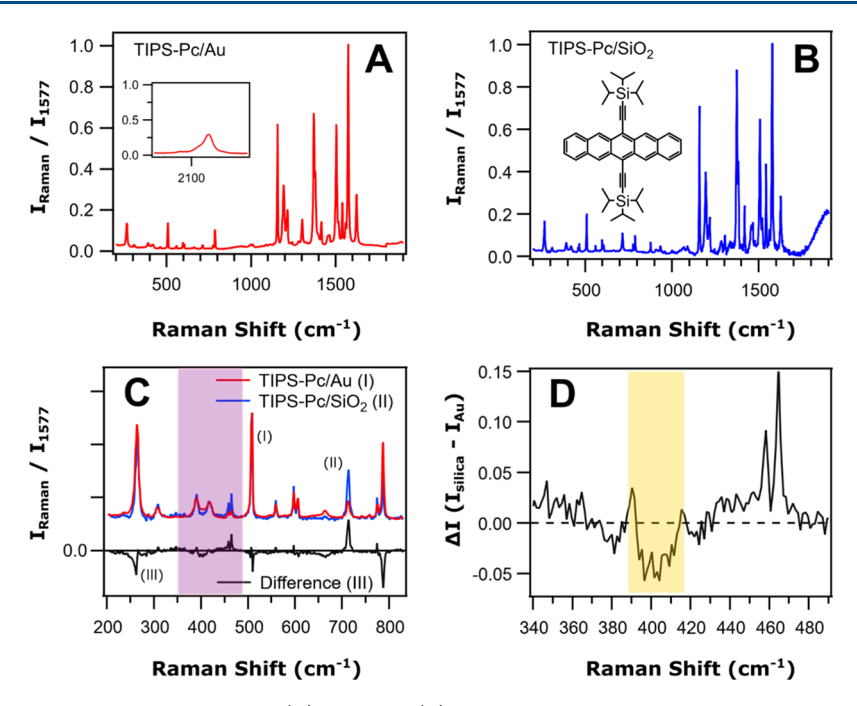


Figure 1. Raman spectra of thick TIPS-Pc films on gold (A) and silica (B) used as a control study. The structure of TIPS-Pc is in Figure 1B. The excitation wavelength is 785 nm, and all spectra are normalized to the 1577 cm<sup>-1</sup> peak intensity. Figure 1A,B shows the range from 200–1900 cm<sup>-1</sup>. The alkyne response is in the inset of Figure 1A. Figure 1C depicts the low-frequency modes of TIPS-Pc on gold (red I), silica (blue II), and the difference spectrum of the two (black III). Figure 1D shows a close-up of the shaded region in 1C. The yellow shaded area highlights the region attributed to the Au–C stretching as discussed in the text.

Raman calculations, the isopropyl groups of TIPS-Pc were modeled using hydrogen atoms to reduce the computational cost, and the Au surface was removed, except for the Au atoms forming Au–C bonds in the chemisorbed system. The replacement of the isopropyl groups with hydrogen atoms is not expected to cause major wavenumber vibrational differences in the whole of TIPS-Pc given that differently functionalized halobenzenes adsorbed to surfaces possess only minor IR vibrational energy differences (less than 20 cm<sup>-1</sup> in C–C stretches and less than 10 cm<sup>-1</sup> in C–H stretches). <sup>55</sup> In all other surface—adsorbate calculations, a full four-layer Au(111) surface and TIPS-Pc with its isopropyl groups were used.

## ■ RESULTS AND DISCUSSION

Studies have shown that molecular orientation and packing on surfaces generated by processing conditions, interfacial interactions, or chemical substitutions can have a profound impact on the resulting charge carrier mobility. Drop casting TIPS-Pc on a substrate, for instance, yields polycrystalline thin films, which is believed to positively influence the charge carrier mobility of these materials based on polaron hopping theory. S7–S9 As nuclear motion can play a vital role in the charge mobility and transport behavior in solid-state semiconductor materials, we use Raman scattering to directly monitor the influence of the substrate on the intermolecular and intramolecular vibrations within the TIPS-Pc thin films.

Substrate Dependence Experiments. We performed a comparative study between gold and silica substrates because of their different conductive nature. Silica is a common dielectric substrate, and it is assumed that no charge transfer occurs between the substrate and the TIPS-Pc film. Conversely, gold is a conductive material, allowing for the possibility of charge transfer between the semiconducting organic film and the substrate. Work by Amy et al. has shown that the photoexcited

pentacene energetics are appropriate for such processes on gold.  $^{60}$  Such interactions can therefore significantly influence the optoelectronic properties of thin films of organic semiconductors.  $^{61}$ 

To determine the influence of the substrate on the vibrations of TIPS-Pc as a film, Raman spectra were collected from 200 to 2300 cm<sup>-1</sup> using an excitation wavelength of 785 nm. This wavelength is off-resonance with the well-documented electronic transitions in solid-state TIPS-Pc to minimize the potential influence of vibronic coupling. 31,62 There is no reported substrate-dependent effect discussed in these studies. Our measurements on a semitransparent 5 nm gold film (not shown) display no major frequency shifts of the lower-energy transition (centered ~700 nm), with the 785 nm excitation being well in the far low-energy tail of the absorption spectrum of the film. The spectra (Figure 1) were normalized to the intensity of the 1577 cm<sup>-1</sup> band. We normalize our spectra to this band because it is both the strongest Raman band observed and does not change in intensity based on the adsorption mechanism. Overall, the unnormalized Raman intensity for the film on gold is enhanced compared to the film on silica (Figure S14 in the Supporting Information). This could be due to the chemical enhancement mechanism (CEM) in Raman scattering or the plasmonic enhancement mechanism. We briefly discuss the arguments for both cases. The CEM enhancement is obtainable in this case via changes in orientation of the adsorbed TIPS-Pc on the gold substrate (vs those in the bulk) altering the polarizability of a given vibrational mode. 63

Additionally, the magnitude of the enhancement is approximate with that of the CEM (10<sup>1</sup> to 10<sup>2</sup> times) as shown in Figure S14 in the Supporting Information. However, there are no reports to our knowledge about the CEM for polyacenes on plasmonic or noble metal surfaces.

Table 1. Electronic Properties of the Physisorbed and Chemisorbed TIPS-Pc/Au(111) Models<sup>a</sup>

system	binding site	BE (eV)	TIPS-pentacene Bader charge (e) <sup>b</sup>	PACDD (e/Å)	Au-C bond distance (Å)	Au-C Mayer bond order	C≡C/C=C bond distance (Å)	C 1s orbital energy (eV)
physisorbed	hollow (H <sub>fcc</sub> )	-6.41	+0.23	15.9	3.26	0.22	1.24	$269.9 (269.5)^d$
chemisorbed	bridge (B)	-6.89	+0.02	18.6	$2.19 (2.07)^c$	$0.84 (0.93)^c$	1.28	270.3

"The binding site of the central pentacene ring and BE (eV), calculated by subtracting the adsorbate and surface energies from the surface—adsorbate system, are given. The positive Bader charge of the TIPS-Pc (e), the electronic charge gained directly between the TIPS-Pc and Au(111) surface from the plane-averaged charge density difference (PACDD) in e/Å, the ethynyl Au–C bond distance (Å), the Au–C Mayer bond order from ADF, and the ethynyl/ethene bond distances (Å) are provided. The C 1s orbital energy is presented for the carbon atom involved in chemisorption in the ethynyl. <sup>b</sup>The Au(111) surface is equal but opposite in Bader charge to the TIPS- Pc Bader charge. <sup>c</sup>Optimized TIPS- Pc model with two Au atoms on the reactive alkyne/alkene carbons instead of an Au(111) surface. <sup>d</sup>Gas-phase C 1s core orbital energy.

Thus, it is also possible that plasmon enhancement due to the ultrathin gold thickness and surface roughness (normally  $10^3$  to  $10^9$  times) was simply less effective as a result of the TIPS-Pc film thickness  $^{63,64}$  and the metallic layer thickness. The plasmonic mechanism solely enhances Raman scattering for molecules in close proximity with said plasmons,  $^{66}$  so a 100 nmthick film would predominately yield Raman scattering from molecules unassociated with the plasmons of the gold substrate. Indeed, this is reflected in our spectra, which are nearly identical to those of previous Raman studies of bulk TIPS-Pc.  $^{67,68}$ 

In general, these Raman results are split into four categories: (1) intermolecular motions and various deformation bands from 200–700 cm<sup>-1</sup>, (2) aromatic C–H bending modes from 775 to 1200 cm<sup>-1</sup>, (3) aromatic C–C/C=C stretching modes from 1250–1650 cm<sup>-1</sup>, and (4) the alkyne stretching mode at ~2120 cm<sup>-1</sup>. The alkyne response is below the signal-to-noise threshold for TIPS-Pc on silica (Figures 1B and S14 in Supporting Information) due to TIPS-Pc fluorescence not being quenched, as opposed to the TIPS-Pc on gold (Figures 1A and S14).

In the low-frequency region (200–700 cm<sup>-1</sup>), we notice a broad feature around 420 cm<sup>-1</sup> (Figure 1D) by taking the difference between the spectra in Figure 1A,B. This feature appears as a dip below unity, as opposed to a positive peak, because the Raman intensities were calculated as TIPS-Pc/SiO<sub>2</sub> minus TIPS-Pc/Au. This broad feature bears characteristics attributable to those reported for Au–C stretching modes in the 370 to 420 cm<sup>-1</sup> region on electrode surfaces, <sup>69–71</sup> clusters, <sup>72</sup> and nanoparticles. <sup>73</sup> This is also analogous to results of a Pt–C bond extramolecular vibration from the previous literature. <sup>74</sup>

Electronic Structure Modeling. To understand the substrate dependence of organic thin films, we modeled the adsorption of TIPS-Pc to Au(111). Both physisorption and chemisorption are possible on gold slabs, with the adsorption type being controlled by the binding site above which the molecule aligns. Physisorption is observed in nearly all structurally optimized systems except those where the alkyne carbons, attached to the silicon atoms in TIPS-Pc, are above top sites of the Au surface. In these instances, the alkynes modify into alkenes and create Au-C bonds. A detailed summary of the computed physisorbed and chemisorbed TIPS-Pc/Au models is shown in Table 1. Physisorption is most preferred above a H<sub>fcc</sub>-binding site for the central pentacene ring. The BE for the chemisorbed model is -6.89 eV while the BE is -6.41eV for the physisorbed model, detailing that Au-C bond formation is favorable to C≡C to C=C bond dissociation.

Our results suggest that if the TIPS-Pc achieves a bridge adsorption site for the central pentacene ring and top adsorption sites for the alkyne carbons attached to the silicon atoms, chemisorption will occur as it is thermodynamically preferred through the BEs. However, with the need to meet multiple preferable adsorption site alignments for the TIPS-Pc to gold, chemisorption is not anticipated to be met for each TIPS-Pc in a complete monolayer, where steric repulsion and molecular spacing considerations must be accounted for. Binding sites necessary for inducing physisorption (Figure 2g) versus chemisorption (Figure 2h) are shown.

Bader charges, plane-averaged charge density difference (PACDD), CDD isosurfaces, bond distances, and bond orders are provided (Table 1 and Figure 2). The Bader charges show that the physisorbed TIPS-Pc transfers 0.23 e to the Au(111) surface; this value is much greater than the 0.02 e transferred to Au(111) by the chemisorbed TIPS-Pc. Charge transfer is more pronounced in the van der Waals-driven physisorption while covalent Au-C bond formation induces less charge transfer. The PACDD (Figure 2a,b) possess a noticeably higher maximum between the surface and molecular adsorbate in the chemisorbed system, indicating large electronic charge density between the molecule and surface in the chemisorbed system and suggestive of the formation of covalent Au-C bonds. Qualitative CDD isosurfaces in Figure 2 highlight a gain of charge directly between the Au-C bond of the chemisorbed model that is absent in the physisorbed model. Furthermore, the CDD suggests that the electronic structure of the TIPS-Pc undergoes much more noticeable charge modification when chemisorbed, supporting stabilization in the Au-C bond formation. The physisorbed TIPS-Pc is calculated to adsorb further away at an Au-C distance of 3.26 Å relative to the chemisorbed TIPS-Pc Au-C bonds formed at shorter distances of 2.19 Å. This closer adsorption distance in the chemisorbed TIPS-Pc results in an Au-C bond order of 0.93, supporting single covalent bond formation, thereby transforming from alkyne to alkene with newly attained organometallic character. The charge gain above Au atoms surrounding the TIPS-Pc, resulting from the charge pillow effect, is larger in the physisorbed versus chemisorbed models. This is rationalized through the PACDD data detailing a larger charge loss underneath the physisorbed adsorbate due to Pauli repulsion. The highest occupied molecular orbital of TIPS-Pc/Au shows evidence of Au-C bonding character whereas the lowest unoccupied molecular orbital displays Au-C antibonding character (see Section S3 of the Supporting Information). Therefore, the computational investigation of TIPS-Pc supports chemisorption over physisorption on Au(111) when the adsorption sites are aligned appropriately Supporting Informa-

**Experimental SERS Findings.** It is important to note that while the gold films are polycrystalline, they are composed of a continuous layer of contiguous islands or grains known to have a dominant (111) facet at the exposed interface while other facets might also be present.<sup>75</sup> Although the computations were

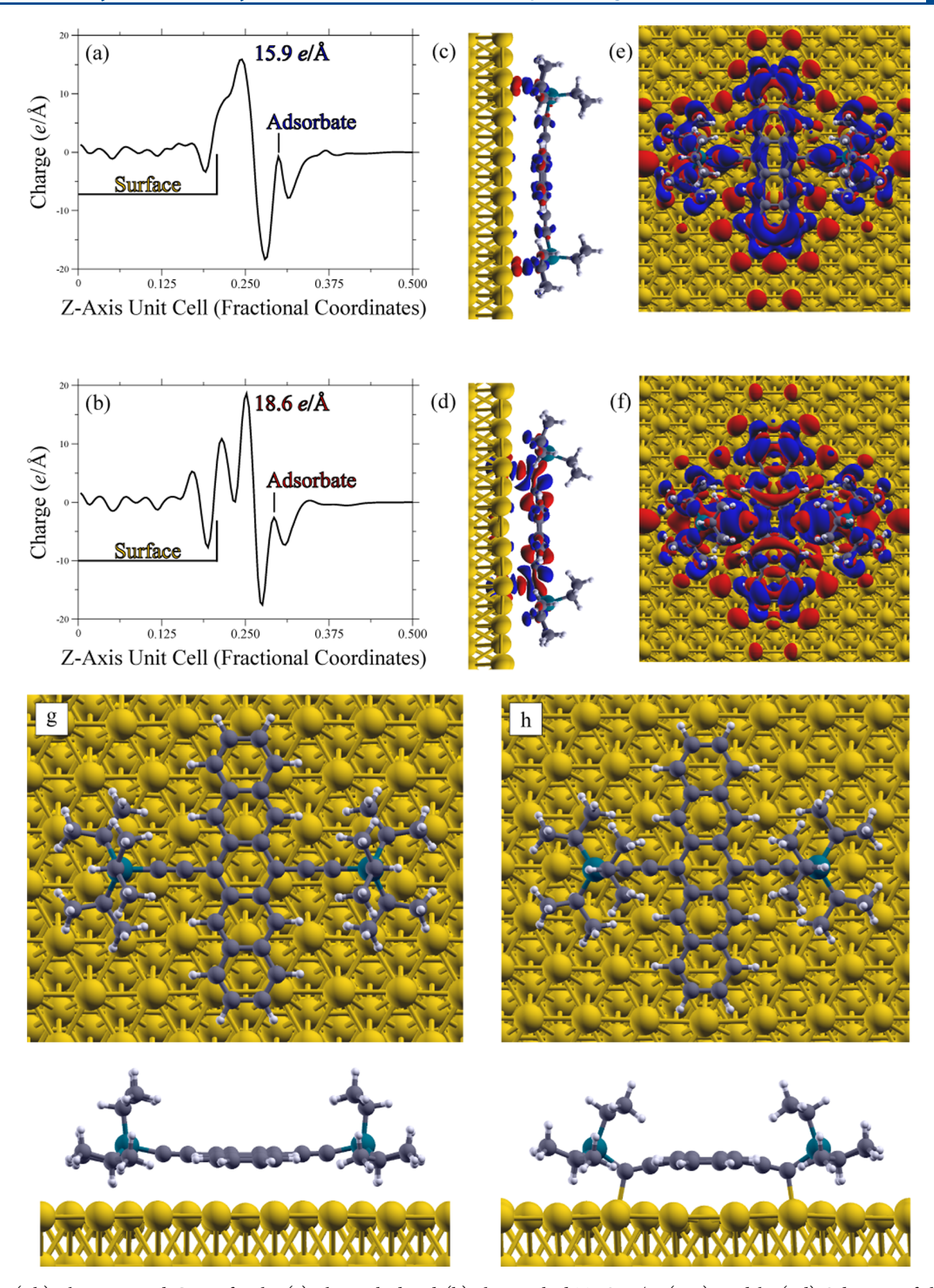


Figure 2. (a,b) Plane-averaged CDDs for the (a) physisorbed and (b) chemisorbed TIPS-Pc/Au(111) models. (c,d) Side view of the CDDs (isovalue =  $\pm 0.01$  e/ų) for the (c) physisorbed and (d) chemisorbed TIPS-Pc/Au(111) models. (e,f) The top-down-view of the CDDs (isovalue =  $\pm 0.003$  e/ų) for the (e) physisorbed and (f) chemisorbed TIPS-Pc/Au(111) models. Electronic charge gain (red) and electronic charge loss (blue) isosurfaces are shown in (c-f). (g,h) Structures for the (g) physisorbed and (h) chemisorbed TIPS-Pc/Au(111) systems. Gold/black/white/teal atoms are Au/C/H/Si.

performed, as a proof of principle, with Au(111), the defect and facet-dependent chemisorption is an important issue out of the scope of this work. To confirm the theoretical findings, we also

used SERS with citrate-capped gold nanorods. Treatment in a UV/ozone cleaner effectively removes the citrate capping ligand after 15 min (Figure S11). Even after 60 min these

nanorods generally maintain their rod shape, although some changes in morphology may appear.<sup>76</sup> There is a slightly reduced SERS enhancement, however, which may be due to slight changes in the morphology of the uncapped nanorods.

This slightly reduced the SERS enhancement (Figure 3). In all UV/ozone treatments and heat treatment (Figure 4), we see

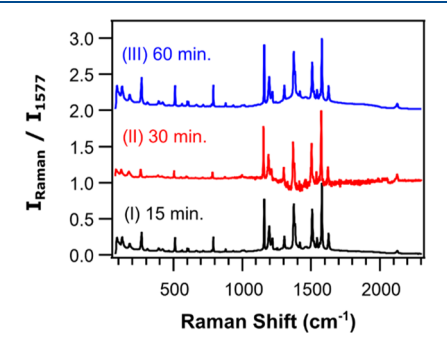


Figure 3. SERS spectra of TIPS-Pc thin films on UV/ozone-treated gold nanorods under 785 nm excitation. Treatments lasted 15 min (black I), 30 min (red II), and 60 min (blue III), respectively. The spectra are vertically offset for clarity.

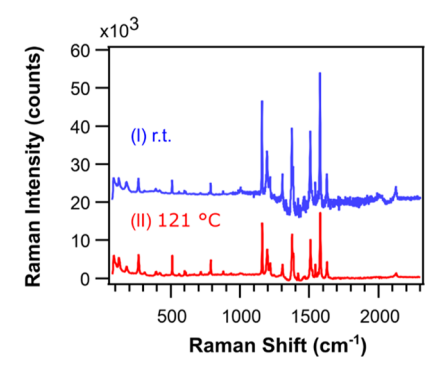


Figure 4. Temperature-dependent film fabrication SERS spectra of TIPS-Pc thin films on gold nanorods under 785 nm excitation at room temperature (blue I) and 121 °C (red II). Gold nanorods were treated with UV/ozone for 30 min prior to the observation. Spectra are offset for clarity.

the alkyne stretching response around 2125 cm<sup>-1</sup> and the Au-C stretching mode around 420 cm<sup>-1</sup>. These responses are expected because all adsorption models calculated refer to monolayer or submonolayer coverages on the gold surface and we do not have that. Indeed, under the current experimental conditions, there should be a minimum of a bilayer on the gold nanorods. Moreover, the chemisorption model only works under specific alignment with a gold surface according to our theoretical models. The nanorods offer a unique scenario, where (111) and (110) are typically the most stable but other surface textures might be present depending on the growth mechanism. Our work is merely meant to show that chemisorption is possible on a gold surface under particular conditions in addition to physisorption. Thus, the presence of an alkyne response does not imply a lack of chemisorption but rather it shows the presence of physisorption.

To further exemplify this point, we performed this measurement again using a 0.05  $\mu$ M solution of TIPS-Pc. This concentration falls below the aggregation concentration for TIPS-Pc such that depositing the chromophore on the gold

nanorods would not lead to multilayer coverage. The results (Figure 5) show first and foremost that there is no alkyne

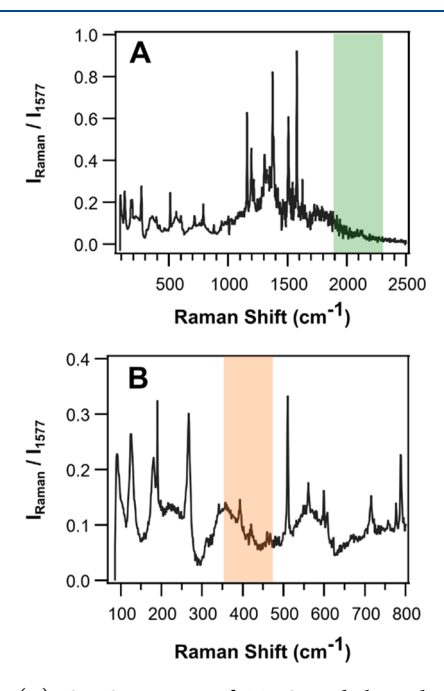


Figure 5. (A) SERS spectra of TIPS-Pc below the aggregate concentration on gold nanorods under 785 nm excitation and (B) close-up of the extramolecular Au−C bond stretching mode at ~420 cm<sup>-1</sup>. Shaded areas are visual guides to the alkyne and Au-C modes, respectively.

response above the noise in Figure 5a. This means that either there is no alkyne moiety present in this TIPS-Pc/gold system or that there are too few to be detected by our instrument (i.e., too low surface coverage to detect). In a chemisorption model, the more peripheral carbon involved in the alkyne bond (the one closer to the silicon atom) covalently bonds to a gold atom and transforms the alkyne into an alkene. However, no additional resolved alkene C=C stretching modes appear in the spectra in Figure 5. This is likely due to near degeneracy of the newly formed alkene stretching mode with the alkene peak observed at about 1620 cm<sup>-1</sup>.

Second, in all cases, the Raman bands at around 420 cm<sup>-1</sup> remain as seen in Figure 5b. This response appears in our calculations in both adsorption models (see Section S2 of the Supporting Information), albeit for nearly degenerate modes. In the chemisorbed model, this mode is attributed to the Au-C stretching mode, calculated closer to 429 cm<sup>-1</sup>, whereas in the physisorbed model, there is a mode attributed to the deformation mode calculated around 400 cm<sup>-1</sup> (see Section S2 of the Supporting Information). Hence, we looked at the difference spectrum in Figure 1C,D which shows a clearly distinguishable broad feature that we attribute to the Au-C extramolecular vibration resonant around 410-420 cm<sup>-1</sup>. This bears resemblance to reported Au-C bands<sup>70</sup> and the extramolecular vibration reported by Humbert et al. corresponding to the formation of a Pt-C bond.<sup>74</sup>

Because there is a vibrational mode in both models in this congested frequency range, all acquired spectra, regardless of sample conditions, yield a signal in this region (see Figures 1-5). According to our calculations (see Section S2 of the Supporting Information), the deformation mode in the physisorption model is not highly polarizable and thus not strongly Ramanactive. In the chemisorption model, the vibrational mode at 420 cm<sup>-1</sup> (429 cm<sup>-1</sup> from DFT-D, see Sections S1 and S2 of the Supporting Information) for the Au–C stretch is highly polarizable and therefore more likely to be observable under the 0.05  $\mu$ M submonolayer coverage condition. In Figure 5B, we still observe a broadened peak at ~420 cm<sup>-1</sup>. Thus, this broadening evidently contains both vibrational modes. Nevertheless, while this feature is not solely conclusive of a chemisorption mechanism, it is compelling when paired with the reduction of the alkyne response.

Interestingly, XPS studies by  $\hat{G}$ noli et al.  $^{38}$  showed that the C 1s spectra displayed two main features at BEs of 284.1 and 283.7 eV (labeled P1 and P2, respectively) and a third weak low BE shoulder (labeled P3), which appeared at 282.8 eV, altogether at lower coverages on Au(111). P2 disappears far above full monolayer coverages and into multilayers while P1 remains most prevalent and P3 gains character. P3 was absent in the case of pentacene and was therefore attributed to the C8 atoms in the TIPS units but specifically on the ethynyl C atom bonded to Si (see Section S4 of the Supporting Information and Table 1). Their vdW-DF-PBE and experimental gas-phase TIPS-Pc XPS spectra agree with one another and support the assignment of P3 to the C8 ethynyl atom and then P1 to the C1-C7 atoms. The isopropyl carbons are attributed to P1 as well. The vdW-DF-PBE simulations involving Au(111) adsorption were not able to describe the P2 band that only emerges upon adsorption experimentally as P2 is not noticeable in the gas-phase spectra. It was therefore assumed that this P2 feature did not derive from the interaction between the Au(111) substrate and isolated adsorbed TIPS-Pc molecules. The origin of the P2 feature in the experimental structure was speculated to be due to a stronger interaction with the surface via defects or to an interaction between TIPS-Pc molecules that was not picked up in theoretical calculations performed on isolated molecules.

Their computed XPS spectra do not explain the lowering of P3 and the emergence of P2 as TIPS-Pc goes from the gas phase to being adsorbed on Au(111) experimentally. The computational structures in their study placed TIPS-Pc in two significantly tilted adaptations relative to the flat Au(111) surface. As a byproduct of these tilted geometries, the ethynyl C8 atom did not significantly interact with the metal. Our parallel TIPS-Pc adsorption model induced strong Au-C chemisorption on the C8 carbon, which increased the C 1s BE by +0.8 eV, being in good agreement with the experimental +0.9 eV difference between the P2 and P3 BEs (see Table 1 and Section S4 of the Supporting Information). If the C8 increase in BE only occurs from Au-C bond formation, then coverages above the monolayer into the multilayer will have a lower percentage of Au-C bonds, resulting in P2 disappearing and P3 emerging, which is exactly what is observed in their experimental XPS spectra. Therefore, we conclude that both P2 and P3 are associated with C8 but with P2 resulting from increased BE in Au-C chemisorption and P3 resulting from free TIPS-Pc. Of note is that Gnoli et al.<sup>38</sup> speculated that P2 could come from a stronger interaction on Au(111) via a surface defect, which is akin to our chemisorbed model as defects would be more reactive.

Figure 6 encompasses all trends in our experimental data that led us to conclude that the molecule is chemisorbed. The top plot in Figure 6 compares the fitted peak intensity of the alkyne peak and the strongest feature at 1577 cm<sup>-1</sup>, which is attributed to a C=C stretching mode along the pentacene long axis.

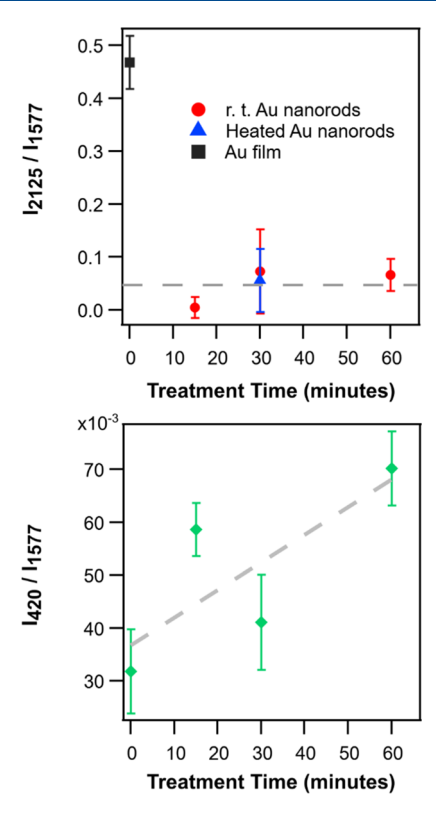


**Figure 6.** Fitted peak intensity ratios of alkyne (top) and Au–C bond (bottom) versus reference peak at 1577 cm<sup>-1</sup>. Time zero is taken from the Figure 1 top spectrum while the remaining times were taken from the respective spectra in Figure 3.

Theoretical Raman spectra display larger-intensity peaks around 1600 cm<sup>-1</sup> in the chemisorbed model versus those in the physisorbed model (see Section S2 in Supporting Information). The black square at time zero represents this intensity ratio for the spectrum acquired in Figure 1A. The red dots are the three UV/ozone treatment durations for the TIPS-Pc-coated gold nanorods. Finally, the blue triangle denotes the heated TIPS-Pc-coated nanorod system. In the bottom plot, the green diamond at time zero denotes the peak intensity ratio of the 420 cm<sup>-1</sup> peak and the 1577 cm<sup>-1</sup> peak for the spectrum acquired in Figure 1. All other times refer to the analogous systems denoted in the top plot as red dots. The heated system is not shown here.

The intensity ratio is helpful in clarifying the absolute Raman response of the vibrational modes of interest. In the first case (top), the intensity of the alkyne response diminishes by a factor of roughly 15 when the gold nanorods are treated for 15 min. The average for the TIPS-Pc film on a gold slide versus the TIPS-Pc-coated nanorods is a factor of 10. No significant differences arise when heated to 121 °C. We deduce that the overall Raman response shown in Figures 1-4 is attributed only to a monolayer or oligolayer of TIPS-Pc on the gold nanorods because the massive plasmon-induced SERS enhancement only applies to those few molecules that feel the plasmons of the nanorods. Thus, we can conclude a significant reduction of alkyne moieties of TIPS-Pc molecules near the gold nanorod surface. Otherwise, the alkyne response should be enhanced equally to the rest of the Raman features depicted above, which it is not. In other words, assuming that there is no modeselective SERS enhancement from the plasmon-induced SERS effect, the lack of alkyne signals is a direct result of a lack of alkyne moieties at the surface, supporting a chemisorption model of adsorption on the gold surface. This observation is supported by our Raman calculations that display no alkyne vibrations in the chemisorbed model that are clearly present during physisorption. Finally, in the submonolayer coverage instance depicted in Figure 5, we calculated a peak intensity ratio for 2125 cm<sup>-1</sup>/1577 cm<sup>-1</sup> of 0.04, which is in agreement with that shown in Figure 6.

In addition to this result, the opposite trend occurs for the  $420~\rm cm^{-1}$  feature, which we attribute to the Au–C stretching mode, relative to the  $1577~\rm cm^{-1}$  C=C stretching mode. Again, in a physisorption model, there would still be a peak at  $\sim$ 420 cm<sup>-1</sup> frequency, attributed to a deformation mode, which explains the presence of said feature in the spectra in Figure 1; however, if there was chemisorption of TIPS-Pc to gold, the Raman intensity of this feature would increase relative to the  $1577~\rm cm^{-1}$  mode. The enhancement is less significant than the alkyne diminution discussed before as the overall average enhancement is only a factor of about 2. Indeed, even in the submonolayer coverage scenario (Figure 5), we calculated a peak intensity ratio for  $420~\rm cm^{-1}/1577~\rm cm^{-1}$  of  $60~\rm x~10^{-3}$ , which is in agreement with that seen in Figure 6 (bottom).

When comparing these results to the results shown in Figure 5, where there is no formation of a multilayer, we deduce that chemisorption occurs. We also note that this adsorption model, while energetically favorable, is only detectable in submonolayer systems and only if there is appropriate alignment between the peripheral alkyne carbon and a gold atom along the surface. This means that there is no immediate way to ensure only one type of adsorption over another, and thus, physisorption and chemisorption both occur in device-applicable systems such as OFETs of photovoltaics.

#### CONCLUSIONS

In summary, we show direct evidence of chemisorption of TIPS-Pc on gold and co-existence of chemisorbed and physisorbed species. The adsorption mechanism of TIPS-Pc plays a vital role in the electronic structure of the chromophore/gold interface. The presence of both adsorption mechanisms in various TIPS-Pc on gold systems was detected using Raman and SERS. Evidence of TIPS-Pc chemisorption was demonstrated through SERS on an unaggregated film of TIPS-Pc, where the Raman response of the alkyne is diminished relative to the reference response at 1577 cm<sup>-1</sup>. The opposite trends also occur as the relative intensity of the Raman peak at 420 cm<sup>-1</sup>, attributed to the Au-C stretching mode, which increases with respect to the reference band at 1577 cm<sup>-1</sup>. Chemisorption does not appear to be the exclusive binding mechanism, thus, some Raman response stems from physisorbed TIPS-Pc as well. This being more prominent for multilayered TIPS-Pc films when stock solutions with concentrations higher than 0.05  $\mu M$  are used. The adsorption geometry and properties of the charge-surface complex at interfaces between donor and acceptor moieties are essential for the overall elucidation of interfacial optoelectronic systems consisting of organic semiconductor/metal devices such as OFETs and organic photovoltaic devices. The adsorption geometry and the strength of the molecule-surface and molecule-molecule interactions define the electronic structure of the system and excitonic dynamics. Practically, this can impact light emission and absorption, charge and energy transport, and charge carrier mobility. Furthermore, studies on OFETs and organic photovoltaics properties would ultimately

determine what adsorption instance is preferable to these technologies.

## ASSOCIATED CONTENT

# Supporting Information

The Supporting Information is available free of charge at https://pubs.acs.org/doi/10.1021/acs.jpcc.1c10283.

Additional data on the optical and SERS particles and characterization data, DFT-simulated IR and Raman spectra for the physisorbed and chemisorbed TIPS-Pc on Au(111), frontier molecular orbitals of the TIPS-Pc/Au chemisorbed model, carbon 1 s core orbital energies, and coordinates for the chemisorbed TIPS-Pc and physisorbed TIPS-Pc (PDF)

# AUTHOR INFORMATION

## **Corresponding Authors**

Daniel P. Miller — Department of Chemistry, Hofstra University, Hempstead, New York 11549, United States; orcid.org/0000-0003-1507-2667;

Email: Daniel.P.Miller@hofstra.edu

Luis Velarde – Department of Chemistry, University at Buffalo, State University of New York, Buffalo, New York 14260-3000, United States; orcid.org/0000-0001-6329-3486; Email: lvelarde@buffalo.edu

#### **Authors**

Brian Breeman – Department of Chemistry, University at Buffalo, State University of New York, Buffalo, New York 14260-3000, United States

Angelo T. Tiglias — Department of Chemistry, Hofstra
University, Hempstead, New York 11549, United States
Joseph Mancuso — Department of Chemistry, Hofstra
University, Hempstead, New York 11549, United States
Eva Zurek — Department of Chemistry, University at Buffalo,
State University of New York, Buffalo, New York 142603000, United States; orcid.org/0000-0003-0738-867X

Complete contact information is available at: https://pubs.acs.org/10.1021/acs.jpcc.1c10283

## **Author Contributions**

The article was written through contributions of all authors. All authors have given approval to the final version of the article.

#### Notes

The authors declare no competing financial interest.

## ACKNOWLEDGMENTS

L.V. and B.B. gratefully acknowledge support from the National Science Foundation under the award number CHE-1900272. D.P.M. acknowledges support from the National Science Foundation CHE-2108597. D.P.M. and E.Z. thank the Center for Computational Research, CCR Facility Description (https://ubir.buffalo.edu/xmlui/handle/10477/79221), for computing support. D.P.M. thanks Luc-Philippe Paulemon and Toon-Chien Wong for assistance in acquiring computing equipment.

## REFERENCES

(1) Jiang, H.; Kammler, M.; Ding, F.; Dorenkamp, Y.; Manby, F. R.; Wodtke, A. M.; Miller, T. F.; Kandratsenka, A.; Bünermann, O. Imaging Covalent Bond Formation by H Atom Scattering from Graphene. *Science* **2019**, *364*, 379–382.

- (2) Borodin, D.; Rahinov, I.; Shirhatti, P. R.; Huang, M.; Kandratsenka, A.; Auerbach, D. J.; Zhong, T.; Guo, H.; Schwarzer, D.; Kitsopoulos, T. N. Following the microscopic pathway to adsorption through chemisorption and physisorption wells. *Science* **2020**, *369*, 1461–1465.
- (3) King, D. A.; Wells, M. G. Reaction Mechanism in Chemisorption Kinetics: Nitrogen on the {100} Plane of Tungsten. *Proc. Roy. Soc. Lond. Math. Phys. Sci.* **1974**, 339, 245–269.
- (4) King, D. A.; Wells, M. G. Molecular Beam Investigation of Adsorption Kinetics on Bulk Metal Targets: Nitrogen on Tungsten. *Surf. Sci.* **1972**, *29*, 454–482.
- (5) Schaefer, S.; Fierro, V.; Szczurek, A.; Izquierdo, M. T.; Celzard, A. P. Chemisorption and Spill-over Contributions to Hydrogen Storage. *Int. J. Hydrogen Energy* **2016**, *41*, 17442–17452.
- (6) Lavrich, D. J.; Wetterer, S. M.; Bernasek, S. L.; Scoles, G. Physisorption and Chemisorption of Alkanethiols and Alkyl Sulfides on Au(111). *J. Phys. Chem. B* **1998**, *102*, 3456–3465.
- (7) Hammer, B. M.; Morikawa, Y.; Nørskov, J. K. CO Chemisorption at Metal Surfaces and Overlayers. *Phys. Rev. Lett.* **1996**, *76*, 2141–2144.
- (8) Ruiz, R. C.; Choudhary, D.; Nickel, B.; Tocoli, T.; Chang, K. C.; Mayer, A. C.; Clancy, P.; Blakely, J. M.; Headrick, R. L.; Iannotta, S.; Malliaras, G. G. Pentacene Thin Film Growth. *Chem. Mater.* **2004**, *16*, 4497–4508
- (9) Jayalatharachchi, V.; MacLeod, J.; Lipton-Duffin, J. Metal Microsubstrates on Si (111): Crystallography, Morphology, and Interactions with a Molecular Adsorbate. *J. Phys. Chem. C* **2021**, 125, 14326–14331.
- (10) Rettner, C. T. M.; Millins, C. B. Dynamics of the Chemisorption of  $O_2$  on Pt(111): Dissociation via Direct Population of a Molecularly Chemisorbed Precursor at High Incidence Kinetic Energy. *J. Chem. Phys.* **1991**, 94, 1626–1635.
- (11) Zambelli, T. B.; Barth, J. V.; Wintterlin, J.; Ertl, G. Complex Pathways in Dissociative Adsorption of Oxygen on Platinum. *Nature* **1997**, 390, 495–497.
- (12) Shirhatti, P. R.; Rahinov, I.; Golibrzuch, K.; Werdecker, J.; Geweke, J.; Altschäffel, J.; Kumar, S.; Auerbach, D. J.; Bartels, C.; Wodtke, A. M. Observation of the adsorption and desorption of vibrationally excited molecules on a metal surface. *Nat. Chem.* **2018**, 10, 592–598.
- (13) Yang, G. F.; Fang, L.; Tan, K.; Shi, S.; Su, Z.; Wang, R. Quantum Chemical Study of Structures, Electronic Spectrum, and Nonlinear Optical Properties of Gold—Pentacene Complexes. *Organometallics* **2007**, *26*, 2082—2087.
- (14) Stern, H. L. C.; Cheminal, A.; Yost, S. R.; Broch, K.; Bayliss, S. L.; Chen, K.; Tabachnyk, M.; Thorley, K.; Greenham, N.; Hodgkiss, J. M.; Anthony, J.; Head-Gordon, M.; Musser, A. J.; Rao, A.; Friend, R. H. Vibronically Coherent Ultrafast Triplet-Pair Formation and Subsequent Thermally Activated Dissociation Control Efficient Endothermic Singlet Fission. *Nat. Chem.* **2017**, *9*, 1205–1212.
- (15) Burdett, J. J.; Gosztola, D.; Bardeen, C. J. The dependence of singlet exciton relaxation on excitation density and temperature in polycrystalline tetracene thin films: kinetic evidence for a dark intermediate state and implications for singlet fission. *J. Chem. Phys.* **2011**, *135*, 214508.
- (16) Wilson, M. W. B. R.; Rao, A.; Clark, J.; Kumar, R. S. S.; Brida, D.; Cerullo, G.; Friend, R. H. Ultrafast dynamics of exciton fission in polycrystalline pentacene. *J. Am. Chem. Soc.* **2011**, *133*, 11830–11833.
- (17) Hanna, M. C. N.; Nozik, A. J. Solar conversion efficiency of photovoltaic and photoelectrolysis cells with carrier multiplication absorbers. *J. Appl. Phys.* **2006**, *100*, 074510.
- (18) Pope, M. S.; Swenberg, C. Electronic Processes in Organic Crystals and Polymers; Oxford Univ. Press, 1999.
- (19) Smith, M. B.; Michl, J. Singlet Fission. Chem. Rev. 2010, 110, 6891-6936.
- (20) Yakutkin, V. A.; Aleshchenkov, S.; Chernov, S.; Miteva, T.; Nelles, G.; Cheprakov, A.; Baluschev, S. Towards the IR Limit of the Triplet-Triplet Annihilation-Supported Up-Conversion: Tetraanthraporphyrin. *Chem.—Eur. J.* **2008**, *14*, 9846–9850.

- (21) Grieco, C. D.; Doucette, G. S.; Munson, K. T.; Swartzfager, J. R.; Munro, J. M.; Anthony, J. E.; Dabo, I.; Asbury, J. B. Vibrational Probe of the Origin of Singlet Exciton Fission in TIPS-Pentacene Solutions. *J. Chem. Phys.* **2019**, *151*, 154701.
- (22) Zhou, Z. M.; Ma, L.; Guo, D.; Zhao, X.; Wang, C.; Lin, D.; Zhang, F.; Zhang, J.; Nie, Z. Ultrafast Dynamics of Long-Lived Bound Triplet Pair Generated by Singlet Fission in 6,13-Bis-(Triisopropylsilylethynyl Pentacene. *J. Phys. Chem. C* **2020**, *124*, 14503–14509.
- (23) Hu, W. S.; Sun, K.; Xu, Q.; Chen, L.; Zhao, Y. Ultrafast Dynamics in Rubrene and Its Spectroscopic Manifestation. *J. Chem. Phys.* **2020**, *153*, 174105.
- (24) Wu, T. N.; Ni, W.; Gurzadyan, G. G.; Sun, L. Singlet Fission from Upper Excited Singlet States and Polaron Formation in Rubrene Film. *RSC Adv.* **2021**, *11*, 4639–4645.
- (25) Sutton, C.; Marshall, M. S.; Sherrill, C. D.; Risko, C.; Brédas, J.-L. The interplay between intramolecular and intermolecular interactions determines the planarization of its tetracene core in the solid state. *J. Am. Chem. Soc.* **2015**, *137*, 8775–8782.
- (26) Eaton, S. W. S.; Shoer, L. E.; Karlen, S. D.; Dyar, S. M.; Margulies, E. A.; Veldkamp, B. S.; Ramanan, C.; Hartzler, D. A.; Savikhin, S.; Marks, T. J.; Wasielewski, M. R. Singlet exciton fission in polycrystalline thin films of a slipstacked perylenediimide. *J. Am. Chem. Soc.* 2013, 135, 14701–14712.
- (27) Cotton, D. E. M.; Moon, A. P.; Roberts, S. T. Using Electronic Sum-Frequency Generation to Analyze the Interfacial Structure of Singlet Fission-Capable Perylenediimide Thin Films. *J. Phys. Chem. C* **2020**, *124*, 11401–11413.
- (28) Lee, J. J.; Jadhav, P.; Reusswig, P. D.; Yost, S. R.; Thompson, N. J.; Congreve, D. N.; Hontz, E.; Voorhis, T. V.; Baldo, M. A. Singlet Exciton Fission Photovoltaics. *Acc. Chem. Res.* **2013**, *46*, 1300–1311.
- (29) Garoni, E. Z.; Zirzlmeier, J.; Basel, B. S.; Hetzer, C.; Kamada, K.; Guldi, D. M.; Tykwinski, R. R. Two-Photon Absorption in Pentacene Dimers: The Importance of the Spacer Using Upconversion as an Indirect Route to Singlet Fission. *J. Am. Chem. Soc.* **2017**, *139*, 14017—14020.
- (30) Walker, B. J. M.; Musser, A. J.; Beljionne, D.; Friend, R. H. Singlet Exciton Fission in Solution. *Nat. Chem.* **2013**, *5*, 1019–1024.
- (31) Kim, H. S. P.; Park, J. H.; Lee, W. H.; Kim, H. H.; Park, Y. D. Tailoring the Crystallinity of Solution-Processed 6,13-Bis-(Triisopropylsilylethynyl)Pentacene via Controlled Solidification. *Soft Matter* **2019**, *15*, 7369–7373.
- (32) Hestand, N. J. Y.; Yamagata, H.; Xu, B.; Sun, D.; Zhong, Y.; Harutyunyan, A. R.; Chen, G.; Dai, H.-L.; Rao, Y.; Spano, F. C. Polarized Absorption in Crystalline Pentacene: Theory vs Experiment. *J. Phys. Chem. C* **2015**, *119*, 22137–22147.
- (33) Tonami, T. N.; Nagami, T.; Okada, K.; Yoshida, W.; Nakano, M. Singlet-Fission-Induced Enhancement of Third-Order Nonlinear Optical Properties of Pentacene Dimers. *ACS Omega* **2019**, *4*, 16181–16190.
- (34) Wilson, M. W. R.; Rao, A.; Ehrler, B.; Friend, R. H. Singlet Exciton Fission in Polycrystalline Pentacene: From Photophysics toward Devices. *Acc. Chem. Res.* **2013**, *46*, 1330–1338.
- (35) Folie, B. D.; Haber, J. B.; Refaely-Abramson, S.; Neaton, J. B.; Ginsberg, N. S. Long-lived correlated triplet pairs in a  $\pi$ -stacked crystalline pentacene derivative. *J. Am. Chem. Soc.* **2018**, *140*, 2326–2335.
- (36) Sharifzadeh, S.; Wong, C. Y.; Wu, H.; Cotts, B. L.; Kronik, L.; Ginsberg, N. S.; Neaton, J. B. Relating the Physical Structure and Optoelectronic Function of Crystalline TIPS-Pentacene. *Adv. Funct. Mater.* **2015**, 25, 2038–2046.
- (37) Dramstad, T. A.; Wu, Z.; Gretz, G. M.; Massari, A. M. Thin Films and Bulk Phases Conucleate at the Interfaces of Pentacene Thin Films. *J. Phys. Chem. C* **2021**, *125*, 16803–16809.
- (38) Gnoli, A.; Ustunel, H.; Toffoli, D.; Yu, L.; Catone, D.; Turchini, S.; Lizzit, S.; Stingelin, N.; Larciprete, R. Bis (triisopropylsilylethynyl) pentacene/Au (111) interface: Coupling, molecular orientation, and thermal stability. *J. Phys. Chem. C* **2014**, *118*, 22522–22532.

- (39) Stein, A.; Maaß, F.; Tegeder, P. Triisopropylsilylethynylpentacene on Au (111): Adsorption properties, electronic structure, and singlet fission dynamics. *J. Phys. Chem. C* **2017**, *121*, 18075–18083.
- (40) Wood, S.; Rigas, G.-P.; Zoladek-Lemanczyk, A.; Blakesley, J. C.; Georgakopoulos, S.; Mas-Torrent, M.; Shkunov, M.; Castro, F. A. Precise characterisation of molecular orientation in a single crystal field-effect transistor using polarised Raman spectroscopy. *Sci. Rep.* **2016**, *6*, 1–8.
- (41) Griffith, O. L.; Anthony, J. E.; Jones, A. G.; Lichtenberger, D. L. Electronic properties of pentacene versus triisopropylsilylethynylsubstituted pentacene: Environment-dependent effects of the silyl substituent. *J. Am. Chem. Soc.* **2010**, *132*, 580–586.
- (42) Kearns, H.; Sengupta, S.; Sasselli, I. R.; Bromley, L., Iii; Faulds, K.; Tuttle, T.; Bedics, M.; Detty, M.; Velarde, L.; Graham, D. Elucidation of the bonding of a near infrared dye to hollow gold nanospheres—a chalcogen tripod. *Chem. Sci.* **2016**, *7*, 5160–5170.
- (43) Rost, M.; Quist, D.; Frenken, J. Grains, growth, and grooving. *Phys. Rev. Lett.* **2003**, *91*, 026101.
- (44) Lee, W. H.; Kim, D. H.; Jang, Y.; Cho, J. H.; Hwang, M.; Park, Y. D.; Kim, Y. H.; Han, J. I.; Cho, K. Solution-processable pentacene microcrystal arrays for high performance organic field-effect transistors. *Appl. Phys. Lett.* **2007**, *90*, 132106.
- (45) Kresse, G. F.; Furthmüller, J. Efficient Iterative Schemes for ab Initio Total-Energy Calculations Using a Plane-Wave Basis Set. *Phys. Rev. B* **1996**, *54*, 11169–11186.
- (46) Perdew, J. P. B.; Burke, K.; Ernzerhof, M. Generalized Gradient Approximation Made Simple. *Phys. Rev. Lett.* **1996**, *77*, 3865–3868.
- (47) Zhang, Y. Y. W. Comment on "Generalized Gradient Approximation Made Simple. *Phys. Rev. Lett.* **1998**, *80*, 890.
- (48) Grimme, S. A.; Antony, J.; Ehrlich, S.; Krieg, H. A Consistent and Accurate Ab Initio Parametrization of Density Functional Dispersion Correction (DFT-D) for the 94 Elements H-Pu. *J. Chem. Phys.* **2010**, *132*, 154104.
- (49) Monkhorst, H. J. P.; Pack, J. D. Special Points for Brillouin-Zone Integrations. *Phys. Rev. B* **1976**, *13*, 5188–5192.
- (50) Blöchl, P. E. Projector Augmented-Wave Method. *Phys. Rev. B* **1994**, *50*, 17953–17979.
- (51) Kresse, G. J.; Joubert, D. From Ultrasoft Pseudopotentials to the Projector Augmented-Wave Method. *Phys. Rev. B* **1999**, *59*, 1758–1775.
- (52) Miller, D. P.; Hooper, J.; Simpson, S.; Costa, P. S.; Tymińska, N.; McDonnell, S. M.; Bennett, J. A.; Enders, A.; Zurek, E. Electronic Structure of Iron Porphyrin Adsorbed to the Pt(111) Surface. *J. Phys. Chem. C.* **2016**, *120*, 29173–29181.
- (53) Te Velde, G. B.; Bickelhaupt, F.; Baerends, E.; Fonseca Guerra, C.; van Gisbergen, S.; Snijders, J.; Ziegler, T. Chemistry with ADF. *J. Comput. Chem.* **2001**, 22, 931–968.
- (54) Van Lenthe, E. B.; Bickelhaupt, E. J. Optimized Slater-Type Basis Sets for the Elements 1-118. *J. Comput. Chem.* **2003**, 24, 1142–1156.
- (55) Schunke, C.; Miller, D. P.; Zurek, E.; Morgenstern, K. Halogen and Structure Sensitivity of Halobenzene Adsorption on Copper Surfaces. *Phys. Chem. Chem. Phys.* **2022.** In print.
- (56) Van Lenthe, E. E.; Ehlers, A. E.; Baerends, E.-J. Geometry optimization in the Zero Order Regular Approximation for relativistic effects. *J. Chem. Phys.* **1999**, *110*, 8943–8953.
- (57) Sharifzadeh, S. W.; Wong, C. Y.; Wu, H.; Cotts, B. L.; Kronik, L.; Ginsberg, N. S.; Neaton, J. B. Relating the Physical Structure and Optoelectronic Function of Crystalline TIPS-Pentacene. *Adv. Funct. Mater.* **2014**, 25, 2038–2046.
- (58) Eggeman, A. S. I.; Illig, S.; Troisi, A.; Sirringhaus, H.; Midgley, P. A. Measurement of Molecular Motion in Organic Semiconductors by Thermal Diffuse Electron Scattering. *Nat. Mater.* **2013**, *12*, 1045–1049
- (59) Jaquith, M. J.; Anthony, J. E.; Marohn, J. A. Long-lived charge traps in functionalized pentacene and anthradithiophene studied by time-resolved electric force microscopy. *J. Mater. Chem.* **2009**, *19*, 6116–6123.

- (60) Amy, F. C.; Chan, C.; Kahn, A. Polarization at the Gold/Pentacene Interface. *Org. Electron.* **2005**, *6*, 85–91.
- (61) Raghuwanshi, V. B.; Bharti, D.; Tiwari, S. P. Flexible Organic Field-Effect Transistors with TIPS-Pentacene Crystals Exhibiting High Electrical Stability upon Bending. *Org. Electron.* **2016**, *31*, 177–182.
- (62) Wu, Y. L.; Liu, K.; Liu, H.; Zhang, Y.; Zhang, H.; Yao, J.; Fu, H. Impact of Intermolecular Distance on Singlet Fission in a Series of TIPS Pentacene Compounds. J. Phys. Chem. Lett. 2014, 5, 3451–3455.
- (63) Theiss, J. P.; Pavaskar, P.; Echternach, P. M.; Muller, R. E.; Cronin, S. B. Plasmonic Nanoparticle Arrays with Nanometer Separation for High-Performance SERS Substrates. *Nano Lett.* **2010**, 10, 2749–2754.
- (64) Hackler, R. A. M.; McAnally, M. O.; Schatz, G. C.; Stair, P. C.; Duyne, R. P. V. Identification of Dimeric Methylalumina Surface Species during Atomic Layer Deposition Using Operando Surface-Enhanced Raman Spectroscopy. *J. Am. Chem. Soc.* **2017**, 139, 2456–2463
- (65) Lee, C.; Robertson, C. S.; Nguyen, A. H.; Kahraman, M.; Wachsmann-Hogiu, S. Thickness of a metallic film, in addition to its roughness, plays a significant role in SERS activity. *Sci. Rep.* **2015**, *5*, 1–10.
- (66) El-Khoury, P. Z.; Schultz, Z. D. From SERS to TERS and Beyond: Molecules as Probes of Nanoscopic Optical Fields. *J. Phys. Chem. C* **2020**, *124*, 27267–27275.
- (67) Xu, J.; Diao, Y.; Zhou, D.; Mao, Y.; Giri, G.; Chen, W.; Liu, N.; Mannsfeld, S. C.; Xue, G.; Bao, Z. Probing the interfacial molecular packing in TIPS-pentacene organic semiconductors by surface enhanced Raman scattering. *J. Mater. Chem. C* **2014**, *2*, 2985–2991.
- (68) Kuramochi, H.; Tahara, T. Tracking Ultrafast Structural Dynamics by Time-Domain Raman Spectroscopy. *J. Am. Chem. Soc.* **2021**, *143*, 9699–9717.
- (69) Berisha, A.; Combellas, C.; Kanoufi, F. d. r.; Médard, J.; Decorse, P.; Mangeney, C.; Kherbouche, I.; Seydou, M.; Maurel, F.; Pinson, J. Alkyl-modified gold surfaces: Characterization of the Au–C bond. *Langmuir* **2018**, *34*, 11264–11271.
- (70) Guo, L.; Ma, L.; Zhang, Y.; Cheng, X.; Xu, Y.; Wang, J.; Wang, E.; Peng, Z. Spectroscopic identification of the Au–C bond formation upon electroreduction of an aryl diazonium salt on gold. *Langmuir* **2016**, *32*, 11514–11519.
- (71) Guttentag, A. I.; Wächter, T.; Barr, K. K.; Abendroth, J. M.; Song, T.-B.; Sullivan, N. F.; Yang, Y.; Allara, D. L.; Zharnikov, M.; Weiss, P. S. Surface structure and electron transfer dynamics of the self-assembly of cyanide on Au {111. *J. Phys. Chem. C* **2016**, *120*, 26736–26746.
- (72) Fielicke, A.; von Helden, G.; Meijer, G.; Pedersen, D. B.; Simard, B.; Rayner, D. M. Gold cluster carbonyls: saturated adsorption of CO on gold cluster cations, vibrational spectroscopy, and implications for their structures. *J. Am. Chem. Soc.* **2005**, *127*, 8416–8423.
- (73) Laurentius, L.; Stoyanov, S. R.; Gusarov, S.; Kovalenko, A.; Du, R.; Lopinski, G. P.; McDermott, M. T. Diazonium-derived aryl films on gold nanoparticles: Evidence for a carbon—gold covalent bond. *ACS Nano* **2011**, *5*, 4219–4227.
- (74) Humbert, C.; Tadjeddine, A.; Busson, B. Sum-Frequency Generation vibrational spectroscopy of an extramolecular chemical bond. *J. Phys. Chem. Lett.* **2011**, *2*, 2770–2773.
- (75) Love, J. C.; Estroff, L. A.; Kriebel, J. K.; Nuzzo, R. G.; Whitesides, G. M. Self-assembled monolayers of thiolates on metals as a form of nanotechnology. *Chem. Rev.* **2005**, *105*, 1103–1170.
- (76) Pang, S. K.; Kurosawa, Y.; Kondo, T.; Kawai, T. Decomposition of Monolayer Coverage on Gold Nanoparticles by UV/ozone Treatment. *Chem. Lett.* **2005**, *34*, 544–545.